

Polarization Microwave Correlation Imaging Method based on Orthogonal Complement Space

Runkun Tian, Dahai Dai*, Penghui Ji, Bo Pang, and Shilong Sun

State Key Laboratory of CEMEE, College of Electronic Science and Technology, National University of Defense Technology, Changsha 410073, China

Email: 18787973696@163.com.

This letter proposes a polarization microwave correlation imaging method based on the orthogonal complement space. It utilizes the orthogonal complement space of the HV antenna radiation field to cross-multiply the echo information, enabling simultaneous correlation imaging and instantaneous polarization measurement of the target. Currently, there is a significant research gap in polarization-driven microwave correlation imaging methods, and the existing relevant studies focus on enhancing the randomness of the radiation field using polarized antenna elements, without incorporating polarization information into the imaging process. Through simulation analysis, this method further improves the quality of microwave correlation imaging and its ability to resist interference. Moreover, under low time-frequency products, the peak sidelobe level (PSL) and isolation (I) of this method are approximately 3.5 dB and 12.5 dB higher, respectively, than those of traditional instantaneous polarization measurement (TIPM) methods.

Introduction: The most commonly used techniques in current radar imaging methods are synthetic aperture imaging and Doppler sharpening. However, these methods rely on Doppler information and have poor imaging performance in the absence of relative motion. In contrast, the novel microwave correlation imaging method does not rely on Doppler information and has high imaging potential, opening up new directions for the development of traditional radar imaging.

Similar to classical optical correlation imaging, microwave correlation imaging is achieved by correlating the highly random radiation field in multiple dimensions with the echo information after radiation interaction with the target to form an image [1-3]. The polarization domain is an important component of describing electromagnetic signals, in addition to the time, space, and frequency domains. However, current research on polarization-driven microwave correlation imaging mainly focuses on using polarized antennas to generate radiation fields [4-6],

ELECTRONICS LETTERS [wileyonlinelibrary.com/iet-el](http://www.wileyonlinelibrary.com/iet-el)

without studying the application of polarization information throughout the entire imaging process. Therefore, this paper proposes a polarization-driven microwave correlation imaging method that utilizes the orthogonal complement space of the HV antenna radiation field to cross-multiply the echo information, and then iteratively images the target using the newly formed correlation equation with the processed radiation field, while simultaneously measuring the instantaneous polarization.

Principle: The microwave correlation forward imaging method used in this paper is based on a frequency hopping radar array. The imaging system operates as shown in Figure 1, where a random frequency hopping antenna array is placed in the working area of the aircraft. Each array element independently generates a random frequency hopping signal, and the superposition of multiple frequency hopping signals forms a random radiation field. The receiving antenna is located in the center of the transmitting antenna array, and the overall operating mode is a multiple-transmit-single-receive mode.

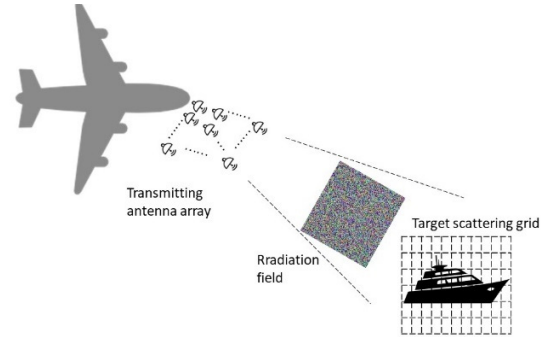


Fig 1 Radar antenna arrangement diagram

Let the vector from the center of the radar array to the target scattering point be denoted as \vec{r} . The M fully polarized transceiving antennas are divided into H antennas and V antennas, which are arranged on both sides of the array. The random frequencies of the two types of antennas are independent of each other and denoted as $f_{Hi}(t)$ and $f_{Vi}(t)$ respectively. The random horizontal polarization angle is denoted as $\gamma_i(t)$, and the random vertical polarization angle is denoted as $\eta_i(t)$. The antenna position vector is denoted as \vec{r}_i . The phase change caused by the random frequency modulation and the distance change between the antenna and the target is defined as $\varphi(f(t), \vec{r}, \vec{r}_i)$. The random radiation fields E_{Hs} and E_{Vs} in the target area, and the target echoes are denoted as E_{Hr} and E_{Vr} [7].

$$\varphi(f(t), \vec{r}, \vec{r}_i) = \exp[-j2\pi f_i(t)(t - |\vec{r} - \vec{r}_i|/c)] \quad (1)$$

$$E_{Hs}(\vec{r}, t) = \sum_{i=1}^M \frac{-f_{Hi}^2(t) E_0 \cos(\gamma_i t)}{4|\vec{r} - \vec{r}_i|^2} \varphi(f_{Hi}(t), \vec{r}, \vec{r}_i) \quad (2)$$

$$E_{Vs}(\vec{r}, t) = \sum_{i=1}^M \frac{-f_{Vi}^2(t) E_0 \sin(\eta) e^{j\eta}}{4|\vec{r} - \vec{r}'|^2} \phi(f_V(t), \vec{r}, \vec{r}_i) \quad (3)$$

$$E_{Hr}(t) = \sum_{i=1}^M \iint \left(\frac{\cos(\gamma_i t) S_{HH}(\vec{r}) + \sin(\eta) e^{j\eta} S_{HV}(\vec{r})}{\sin(\eta) e^{j\eta} S_{HV}(\vec{r})} \right) \times Er' d\vec{r} \quad (4)$$

$$E_{Vr}(t) = \sum_{i=1}^M \iint \left(\frac{\cos(\gamma_i t) S_{VH}(\vec{r}) + \sin(\eta) e^{j\eta} S_{VV}(\vec{r})}{\sin(\eta) e^{j\eta} S_{VV}(\vec{r})} \right) \times Er' d\vec{r} \quad (5)$$

$$Er' = \frac{-\sigma(\vec{r}) f_{Hi}^2(t) E_0}{4|\vec{r} - \vec{r}'|^2} \phi(f_V(t), \vec{r}, \vec{r}_i) \quad (6)$$

The relationship can be obtained as shown in Equation (6), and through inversion, the scattering characteristics and polarization scattering characteristics of the target can be obtained.

$$\begin{bmatrix} E_{Hr} \\ E_{Vr} \end{bmatrix} = \begin{bmatrix} S_{HH} & S_{HV} \\ S_{VH} & S_{VV} \end{bmatrix} \begin{bmatrix} \sigma E_{Hs} \\ \sigma E_{Vs} \end{bmatrix} \quad (7)$$

To solve the above equation, the optimal scenario is for the HV antenna radiation fields to be mutually orthogonal [8]. However, the radiation field in microwave correlation imaging is random and uncontrollable. Even if tools such as masks are used to directly generate the radiation field, it cannot be guaranteed that the HV radiation fields at the target are mutually orthogonal. Therefore, an auxiliary matrix must be used to process the HV radiation fields. First, the radiation field matrix of the target is subjected to QR decomposition to obtain the orthogonal complement spaces E_{Hsb} and E_{Vsb} of the radiation field matrices E_{Hs} and E_{Vs} . Therefore, multiplying the target HV echoes with the orthogonal complement spaces of the HV radiation fields yields:

$$\begin{cases} E_{Hsb} E_{Hr} = E_{Hsb} E_{Hs} S_{HH} + E_{Hsb} E_{Vs} S_{HV} \\ E_{Vsb} E_{Hr} = E_{Vsb} E_{Hs} S_{HH} + E_{Vsb} E_{Vs} S_{HV} \\ E_{Hsb} E_{Vr} = E_{Hsb} E_{Hs} S_{VH} + E_{Hsb} E_{Vs} S_{VV} \\ E_{Vsb} E_{Vr} = E_{Vsb} E_{Hs} S_{VH} + E_{Vsb} E_{Vs} S_{VV} \end{cases} \quad (8)$$

The correlation equation can be solved using the properties of the orthogonal complement matrix, as shown in Equation (8), enabling the imaging of the target and the measurement of the target's instantaneous polarization scattering matrix.

Simulations: Simulations were performed using data from polarimetric SAR images of a ship on the sea surface [9]. First, the target observation area was divided into a scattering point grid. The imaging area of $40\text{m} \times 40\text{m}$ was divided into 1600 imaging grids of $1\text{m} \times 1\text{m}$ each. The simulated target is shown in Figure 2(a). The spatial correlation of the radiation field for a single pulse of the H antenna is shown in Figure 2(b), and Figure 2(c) shows the results of classical microwave correlation imaging (CMCI).

Figure 2(d) shows the results of polarization microwave correlation imaging (PMCI). In this simulation, four points were randomly selected from the imaging results to analyze the errors of the instantaneous polarization measurement matrix. The measurement results are shown in Table 1.

Table 1. Measured results of target polarimetric scattering matrix.

	Target scattering	Imaging computation	Error rate
1	$\begin{bmatrix} 0.3897 & -0.3658 \\ 0.9004 & -0.9311 \end{bmatrix}$	$\begin{bmatrix} 0.3892 & -0.3623 \\ 0.9078 & -0.9278 \end{bmatrix}$	0.8%
2	$\begin{bmatrix} -0.4462 & -0.9077 \\ -0.8057 & 0.6469 \end{bmatrix}$	$\begin{bmatrix} -0.4464 & -0.9035 \\ -0.7968 & 0.6436 \end{bmatrix}$	0.3%
3	$\begin{bmatrix} 0.9150 & 0.9298 \\ -0.6848 & 0.9412 \end{bmatrix}$	$\begin{bmatrix} 0.9166 & 0.9395 \\ -0.6770 & 0.9484 \end{bmatrix}$	0.84%
4	$\begin{bmatrix} 0.9143 & -0.0292 \\ 0.6006 & -0.7162 \end{bmatrix}$	$\begin{bmatrix} 0.9170 & -0.0385 \\ 0.6020 & -0.7180 \end{bmatrix}$	0.2%

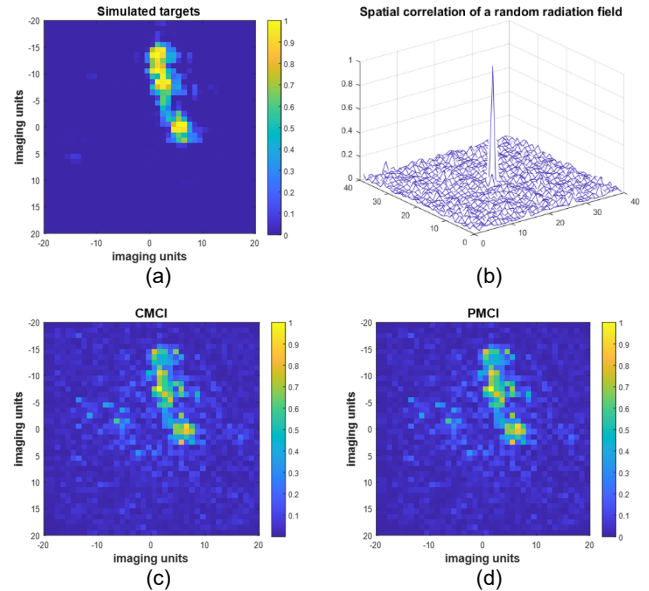


Fig 2 PMCI simulation figures: (a) Simulated target; (b) Spatial autocorrelation of H antenna radiation field; (c) CMCI; (d) PMCI

From Figure 2, it can be observed that PMCI accurately locates the target, and the color intensity in the images represents the sum of the square of the target's S matrix, which is consistent with the target. From Table 1, it can be seen that there is a slight error in the measured target polarization scattering matrix. The error rate was evaluated by calculating the difference in Euclidean distance between the actual and imaging values of the target's polarization matrix, with an average error rate of 0.535%, indicating the reliability of the measurement results. This method enables simultaneous imaging of the target and measurement of the instantaneous polarization matrix.

Evaluation: Under the condition of pulse width $\tau = 0.2\mu\text{s}$ and $0.5\text{GHz} < B < 2.5\text{GHz}$, the measurement results of the two radiation fields PSL and I of the HV antenna are obtained [10], as shown in Figure 3(a). When $B\tau < 380$, the average PSL and I of the two signals from the HV antenna using this method are approximately 13dB and 3dB higher than those of the classical method using positive and negative linear frequency modulation signals. The different trends of the curves in Figure 3(a) are due to the inherent high randomness of microwave correlation imaging in the time and frequency domains. Therefore, the change in time-frequency product has a small impact on the randomness of the radiation field, with a variation amplitude of less than 0.4dB within the total time-frequency product range ($100 < B\tau < 500$). Therefore, it can be concluded that under low time-frequency product conditions, PMCI has a greater advantage in instantaneous polarization measurement compared to TIPM.

From Figure 3(b), it can be observed that the PMCI method has stronger anti-interference ability in the presence of white noise interference. This is because the correlation imaging part of this method calculates the target's polarization scattering matrix simultaneously with the imaging, which is equivalent to multiple corrections of the correlation calculation results, effectively reducing the impact of interference. At the same time, the simulation did not consider the influence of the polarization antenna itself on noise interference. In practical applications, since the polarization antenna can only receive signals in its polarization direction, the anti-interference ability will be even stronger.

Conclusion: This letter proposes a novel microwave correlation imaging method that simultaneously measures the polarization matrix during imaging. Comparing this new microwave correlation imaging method with traditional methods, it exhibits outstanding advantages in terms of anti-jamming capability and imaging quality. Additionally, in terms of instantaneous polarization measurement, this method achieves higher peak sidelobe level and isolation ratio compared to TIPM, even under low time-frequency products, resulting in better performance. Currently, this method successfully combines microwave correlation imaging with polarization information utilization, further expanding the development of microwave correlation imaging methods in the polarization domain.

Author contributions: Runkun Tian: Conceptualization, data curation, formal analysis, methodology and writing-original draft. Dahai Dai: Supervision, funding acquisition, validation, and. Penghui Ji: Data curation, writing-review. Bo Bang: editing, software, Supervision. Shilong Sun: project administration, Supervision.

Acknowledgements: This work was supported by The National Natural Science Foundation of China under Grant

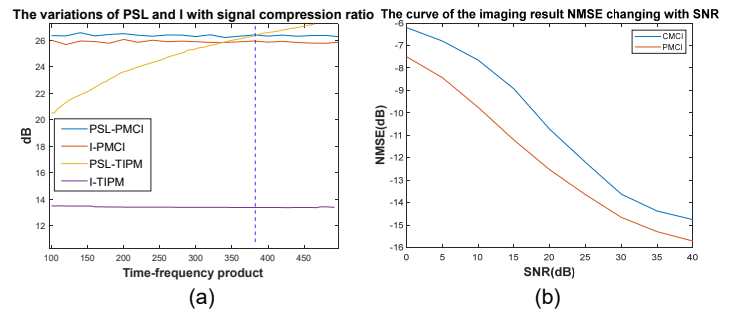


Fig 3 Evaluation of PMCI: (a) PSL and I evaluation, (b) Anti-noise ability evaluation.

62001485, Natural Science Foundation of Hunan Province under Grant 2021JJ40689.

Conflict of interest statement: The authors declare no conflicts of interest.

Data availability statement: Data available on request from the authors

References

- [1] Liu, W., Sun, S., Hu, H., & Lin, H.: Progress and prospect for ghost imaging of moving objects. *Laser & Optoelectronics Progress*. 58(10), 1011001(2021)
- [2] Cheng, Y., Zhou, X., Xu, X., Qin, Y., & Wang, H.: Radar coincidence imaging with stochastic frequency modulated array. *IEEE Journal of Selected Topics in Signal Processing*. 11(2), 414-427 (2016)
- [3] Quan, Y., Zhang, R., Li, Y., Xu, R., Zhu, S., & Xing, M.: Microwave correlation forward-looking super-resolution imaging based on compressed sensing. *IEEE Transactions on Geoscience and Remote Sensing*. 59(10), 8326-8337 (2021)
- [4] Li, L., Wang, S. Y., Chen, J., Zhang, C., Tang, J., & Su, T.: A circular - polarized and high - gain microwave correlation imaging antenna based on rotating elements. *International Journal of RF and Microwave Computer - Aided Engineering*, 32(12), e23497(2022)
- [5] Abou-Khousa, M. A., Rahman, M. S. U., & Xingyu, X.: Dual-polarized microwave imaging probe. *IEEE Sensors Journal*, 19(5), 1767-1776(2018)
- [6] Zhu, S., Dong, X., He, Y., Zhao, M., Dong, G., Chen, X., & Zhang, A.: Frequency-polarization-diverse aperture for coincidence imaging. *IEEE Microwave and Wireless Components Letters*, 28(1), 82-84(2017)
- [7] Ying, K., Yu, X., Shen, J., Zhang, S., & Guo, Y.: Intelligent Microwave Staring Correlated Imaging. *Progress In Electromagnetics Research*, 176, 109-128(2023)
- [8] Shen, B., Liu, T., Liu, W., & Gao, G.: Simultaneous Polarization Measurement and High-Resolution Imaging Algorithm Inspired by Bat Sound Waveform. *IEEE Journal on Miniaturization for Air and Space Systems*, 3(4), 264-275(2022)
- [9] Wang, Y., Wang, C., Zhang, H., Dong, Y., & Wei, S.: A SAR dataset of ship detection for deep learning under complex backgrounds. *remote sensing*, 11(7), 765(2019)
- [10] Fu, X., Yan, H., Zhao, L., Wang, C., & Gao, M.: Channel isolation and range sidelobe suppression for instantaneous full-polarization radar. In *International Conference on Information Science and Technology* (pp. 689-693). IEEE (2011)